The EMBO Journal (2007) 26, 3836–3846 | © 2007 European Molecular Biology Organization | All Rights Reserved 0261-4189/07
www.embojournal.org

THE EMBO JOURNAL

Tertiary structure and function of an RNA motif required for plant vascular entry to initiate systemic trafficking

Xuehua Zhong[1,3], Xiaorong Tao[1,3], Jesse Stombaugh[2], Neocles Leontis[2,*] and Biao Ding[1,*]

[1]Department of Plant Cellular and Molecular Biology and Plant Biotechnology Center, Ohio State University, Columbus, OH, USA and [2]Department of Chemistry and Center for Biomolecular Sciences, Bowling Green State University, Bowling Green, OH, USA

Vascular entry is a decisive step for the initiation of long-distance movement of infectious and endogenous RNAs, silencing signals and developmental/defense signals in plants. However, the mechanisms remain poorly understood. We used *Potato spindle tuber viroid* (PSTVd) as a model to investigate the direct role of the RNA itself in vascular entry. We report here the identification of an RNA motif that is required for PSTVd to traffic from nonvascular into the vascular tissue phloem to initiate systemic infection. This motif consists of nucleotides U/C that form a water-inserted *cis* Watson–Crick/Watson–Crick base pair flanked by short helices that comprise canonical Watson–Crick/Watson–Crick base pairs. This tertiary structural model was inferred by comparison with X-ray crystal structures of similar motifs in rRNAs and is supported by combined mutagenesis and covariation analyses. Hydration pattern analysis suggests that water insertion induces a widened minor groove conducive to protein and/or RNA interactions. Our model and approaches have broad implications to investigate the RNA structural motifs in other RNAs for vascular entry and to study the basic principles of RNA structure–function relationships.

The EMBO Journal (2007) **26,** 3836–3846. doi:10.1038/sj.emboj.7601812; Published online 26 July 2007
Subject Categories: RNA; plant biology
Keywords: phloem; RNA motif; RNA structure; RNA trafficking; viroid

Introduction

Increasing evidence indicates that intercellular trafficking of RNAs plays important roles in physiological and developmental processes in plants (Ruiz-Medrano *et al*, 1999; Kim *et al*, 2001; Haywood *et al*, 2005; Banerjee *et al*, 2006; Lough and Lucas, 2006). Furthermore, viroid and viral RNAs apparently utilize the endogenous trafficking system to spread within a plant to establish systemic infection (Flores *et al*, 2005; Lucas, 2006; Ding and Itaya, 2007). Gene silencing signals, which likely have an RNA component, traffic intercellularly to trigger systemic silencing in plants (Palauqui *et al*, 1997; Voinnet and Baulcombe, 1997; Voinnet *et al*, 1998; Yoo *et al*, 2004), *Caenorhabditis elegans* (Fire *et al*, 1998) and Tribolium (Coleoptera) (Bucher *et al*, 2002). These observations suggest that intercellular trafficking of RNAs plays critical roles in many aspects of biology. Elucidating the underlying mechanisms is crucial to understand gene regulation as well as host-pathogen interactions at the organismal level.

Plasmodesmata and the vascular tissue phloem form continuous cytoplasmic channels for direct cell-to-cell and systemic transport of RNAs and proteins as well as photoassimilates in plants (Lucas *et al*, 1993, 2001; Lough and Lucas, 2006). Some plant proteins bind RNAs and facilitate their intercellular trafficking (Xoconostle-Cázarés *et al*, 1999; Yoo *et al*, 2004). Viral proteins play an important role in viral cell-to-cell movement (Lucas, 2006). There is also evidence suggesting that some viral RNAs have a role in systemic infection (Ding *et al*, 2005; Lough *et al*, 2006). In general, the specific role of an RNA, as well as the mechanisms of protein–RNA interactions in trafficking remain poorly understood. In particular, there is little knowledge of how an RNA or protein enters the phloem, which is a decisive step to initiate systemic trafficking (Ding, 1998; Lucas *et al*, 2001; Haywood *et al*, 2002; Lough and Lucas, 2006).

Viroids provide simple models to investigate the direct role of RNA motifs in systemic RNA trafficking. These single-stranded, circular and non-coding RNAs are the smallest pathogens known to date, with sizes ranging from 250 to 400 nucleotides (Flores *et al*, 2005; Ding and Itaya, 2007). We utilize *Potato spindle tuber viroid* (PSTVd) as our experimental system. This viroid contains 359 nucleotides and forms a rod-like secondary structure in its native *in vitro* state (Figure 1A; Gross *et al*, 1978). There is strong evidence that this structure exists and functions *in vivo* (Wassenegger *et al*, 1994; Zhong *et al*, 2006; Eiras *et al*, 2007; Wang *et al*, 2007). PSTVd replicates in the nucleus via a rolling-circle mechanism, which starts with transcription of the incoming monomeric, circular (+)-strand RNA into multimeric, linear (−)-strands. The latter then serve as the replication intermediates for the production of multimeric, linear (+)-strands that are finally processed into unit-length, circular RNAs (Branch and Robertson, 1984). To establish systemic infection, PSTVd traffics across many different cellular boundaries from the epidermis to the phloem, to spread throughout the infected plant (Figure 1B; Ding *et al*, 2005; Ding and Itaya, 2007). Because PSTVd does not encode proteins, it must have evolved sequence/structural features that are

*Corresponding authors. B Ding, Department of Plant Cellular and Molecular Biology and Plant Biotechnology Center, Ohio State University, Columbus, OH 43210, USA. Tel.: +1 614 247 6077; Fax: +1 614 292 5379; E-mail: ding.35@osu.edu or N Leontis, Department of Chemistry and Center for Biomolecular Sciences, Bowling Green State University, Bowling Green, OH 43404, USA.
Tel.: +1 419 372 8663; Fax: +1 419 372 9809; E-mail: leontis@bgnet.bgsu.edu
[3]These authors contributed equally to this work

Received: 24 April 2007; accepted: 2 July 2007; published online: 26 July 2007

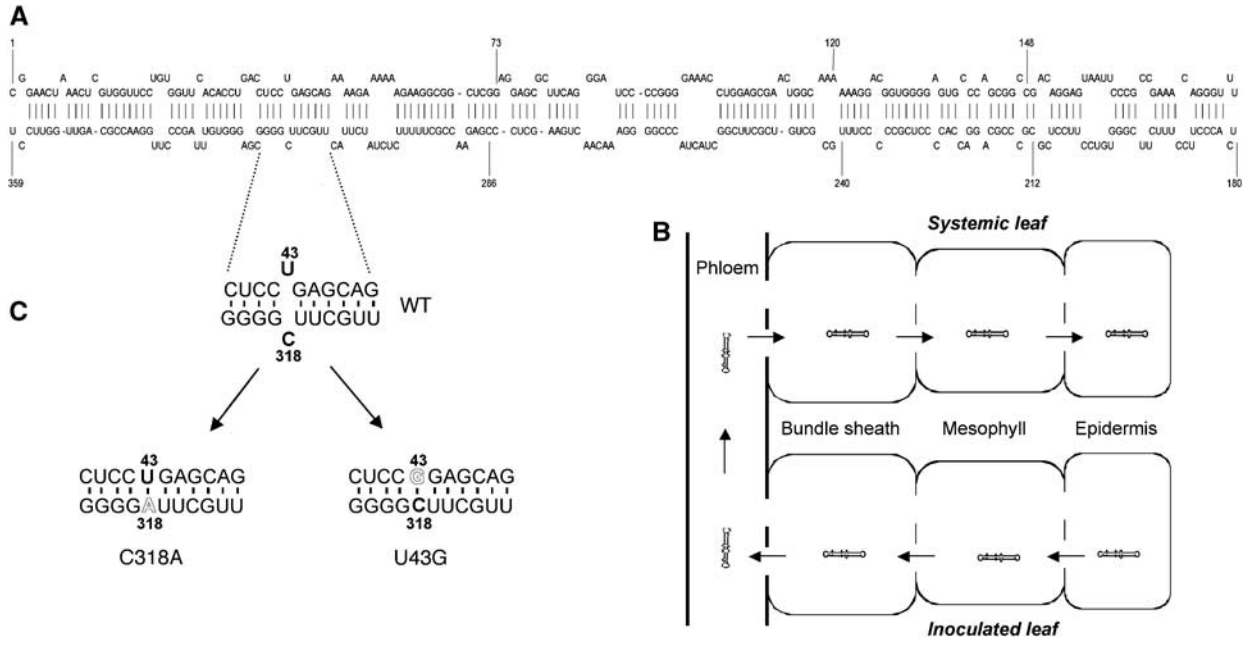

Figure 1 Mutational analysis of PSTVd systemic infection. (**A**) A schematic representation of secondary structure of PSTVd, showing genomic location of the U43/C318 'loop' required for systemic infection. (**B**) A schematic representation showing the major cellular boundaries in inoculated and systemic leaves that PSTVd traffics through to establish systemic infection. The open spaces in the lines represent plasmodesmata. The arrows indicate direction of trafficking. For simplicity, the specific cell types in the phloem are not illustrated. (**C**) Enlarged view of nucleotide sequences of the short helices flanking the U43/C318 'loop' in the WT, C318A and U43G mutants.

directly recognized by the endogenous cellular machinery to accomplish replication and systemic trafficking. Therefore, investigating PSTVd structural motifs for trafficking can help shed some light on the general principles of molecular interactions that control systemic RNA trafficking. Using PSTVd as a model, Qi *et al* (2004) presented genetic evidence for the role of an RNA motif in mediating RNA trafficking across a specific cellular boundary in the non-vascular tissue. However, the tertiary structure and functional mechanism of this motif remain to be elucidated.

Here, we report the first loss-of-function genetic identification of an RNA tertiary structural motif in the PSTVd required for vascular entry, specifically from the bundle sheath into the phloem regardless of the developmental stage of an infected leaf. Our results support the hypothesis that tissue-specific factors interact with distinct RNA motifs to control trafficking across specific cellular boundaries. Furthermore, our approach should have broad implications to investigate the structural motifs in endogenous and infectious RNAs critical for vascular entry and to study the basic principles of RNA structure–function relationships.

Results

PSTVd infection of Nicotiana benthamiana as an experimental system

We used infection of *N. benthamiana* by the intermediate strain of PSTVd (WT) as our experimental system. PSTVd replicates efficiently in cultured cells of *N. benthamiana* (Qi and Ding, 2002) and readily establishes systemic infection in the plant (Hu *et al*, 1997; Zhu *et al*, 2001), making it possible to investigate separately structural motifs involved in the replication and trafficking. To establish the system, we used RNA blots to analyze the accumulation of the (+)-circular and linear viroid RNAs in the youngest systemic leaves at 0, 6, 9, 12, 15, 18, 21, 24 and 27 days post inoculation (dpi). As shown in Figure 2A and B, accumulation of the (+)-circular PSTVd in systemic leaves was first visible at 12 dpi. The level reached a maximum around 21 dpi and dropped slightly afterwards. This time course set the basis for the subsequent trafficking experiments.

Identification of PSTVd mutants defective in systemic trafficking

Numerous PSTVd mutations have minimal or drastic effects on infection in tomato (Hammond and Owens, 1987; Loss *et al*, 1991; Qu *et al*, 1993; Hu *et al*, 1996; Owens *et al*, 1991, 1995, 1996). We developed a simple and fast assay to screen for PSTVd mutants that are defective in systemic trafficking. We generated many of these mutants and tested their systemic infection in *N. benthamiana*. Several mutants showed accumulation in inoculated leaves but not in systemic leaves (X Zhong and B Ding, unpublished data). One such mutant contains a C318 to A substitution (C318A) that closes the original U43/C318 'loop' by allowing the formation of a canonical *cis* Watson–Crick/Watson–Crick U43/A318 base pair, without altering the global secondary structure of the viroid RNA, as predicted by mfold (Zuker, 2003; Figure 1C; Supplementary Figure 1). As shown in Figure 3A, the mutant C318A did not accumulate in systemic leaves at 21 dpi. However, it accumulated in the inoculated leaves (Figure 3B). To further determine its replication capacity, we performed replication assays in protoplasts prepared from cultured cells of *N. benthamiana*. As shown in Figure 3C, mutant C318A accumulated in the protoplasts at 3 dpi. Sequencing confirmed maintenance of the mutant sequence in the RNA progeny in the infected prtoplasts and leaves. These data indicate that mutant C318A is

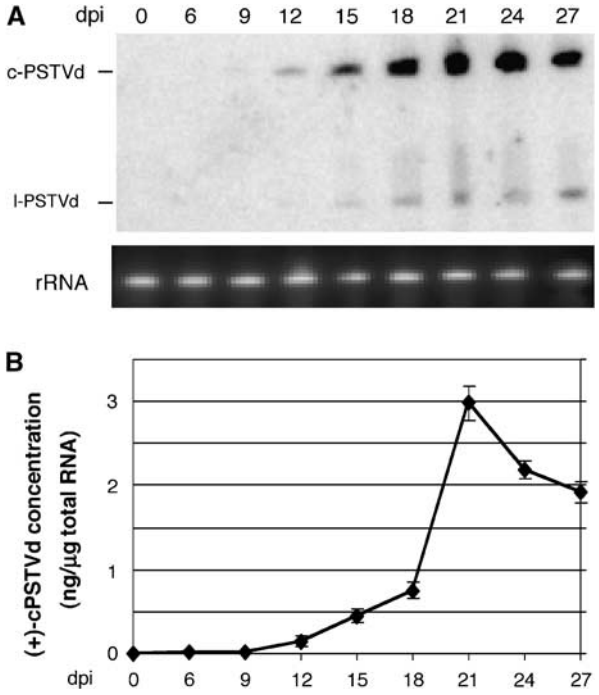

Figure 2 Time course for PSTVd systemic infection in *N. benthamiana* plant. (**A**) RNA blots showing accumulation of both the (+)-circular (c-PSTVd) and linear (l-PSTVd) viroid RNAs at successive dpi. rRNA serves as loading control. (**B**) Quantification of the accumulation levels of c-PSTVd from RNA blot results, calculated by using the known amounts of loading size markers in the same gel as references. Each data point represents the mean value of three biological replicates.

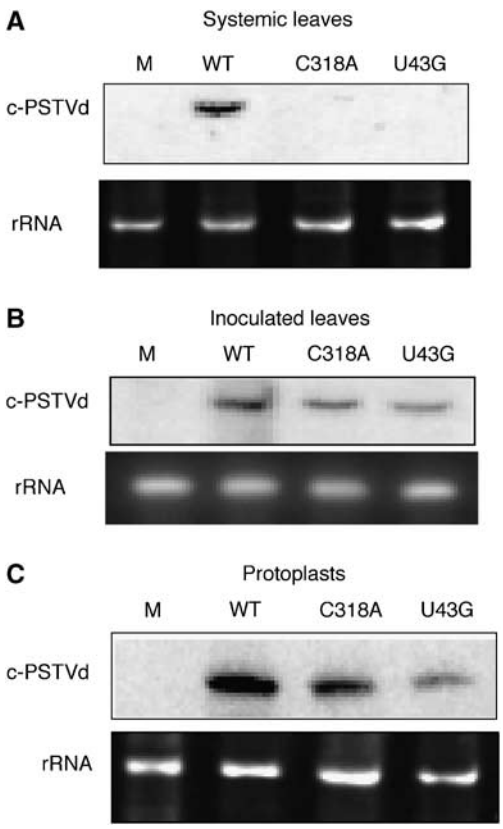

Figure 3 RNA blots showing defects of C318A and U43G mutants in systemic infection in *N. benthamiana*. (**A**) Accumulation of WT, but not the two mutants, in systemic leaves. (**B**) Accumulation of the two mutants as well as the WT in inoculated leaves. (**C**) Accumulation of the two mutants as well as the WT in infected protoplasts. rRNA shows loading control. c-PSTVd, (+)-circular PSTVd; M, mock control.

defective in systemic trafficking rather than replication. Further analyses showed that the mutant did not show accumulation in systemic leaves up to 7 weeks post-inoculation (data not shown), indicating that systemic trafficking of this mutant is abolished rather than delayed.

To further test whether it is the U43/C318 'loop', or the requirement of C at position 318, that is critical for systemic trafficking, we substituted U43 with G to close the 'loop' (Figure 1C), and tested its effect on systemic infection. As shown in Figure 3A and B, mutant U43G was absent from systemic leaves but accumulated in inoculated leaves. U43G also replicated in the protoplasts, albeit at reduced levels compared with the wild type (WT) (Figure 3C). As shown below, this level of reduced accumulation was not the cause for defects in systemic infection. The data provide additional evidence that the U43/C318 'loop' is critical for systemic trafficking of PSTVd in *N. benthamiana*.

Mutants C318A and U43G were capable of trafficking between non-vascular cells

To establish systemic infection, PSTVd inoculated into leaf epidermal cells must be capable of replication and movement into mesophyll, bundle sheath and phloem, followed by long-distance movement through the vascular system and finally exit from the phloem to invade new tissues (Figure 1B). Failure of trafficking at any of these steps will block systemic infection. To identify the cellular interface(s) at which trafficking is blocked for mutants C318A and U43G, we performed *in situ* hybridization experiments to visualize their cellular localization in inoculated leaves. Time points of 6, 12 and 18 dpi were chosen because the accumulation of the WT viroid RNA was first visible in systemic leaves at 12 dpi (Figure 2).

The results from 12 dpi samples are shown in Figure 4 and those from 6 and 18 dpi are shown in Supplementary Figures 2 and 3. At 12 dpi, we could detect the accumulation of mutants C318A and U43G, as well as the WT, in the mesophyll cells (Figure 4A) and in the epidermis (data not shown). Often clusters of cells containing hybridization signals were detected. Identical results were obtained from 6 and 18 dpi samples (Supplementary Figures 2 and 3). These results indicate that the mutant viroid RNAs were capable of trafficking between epidermal and mesophyll cells.

Mutants C318A and U43G failed to traffic from bundle sheath into phloem

As shown in Figure 4B and Supplementary Figures 2 and 3, we could also detect the presence of mutants C318A and U43G, as well as the WT, in the bundle sheath. Strikingly, while the WT viroid RNA was further detected in the phloem cells, the two mutants were never detected there. The same observations also applied to leaf samples collected at 6 and 18 dpi, indicating that blockage of vascular entry for the mutants was maintained during leaf growth.

It is possible that mutants C318A and U43G did enter the phloem and trafficked along the phloem, but at a level below

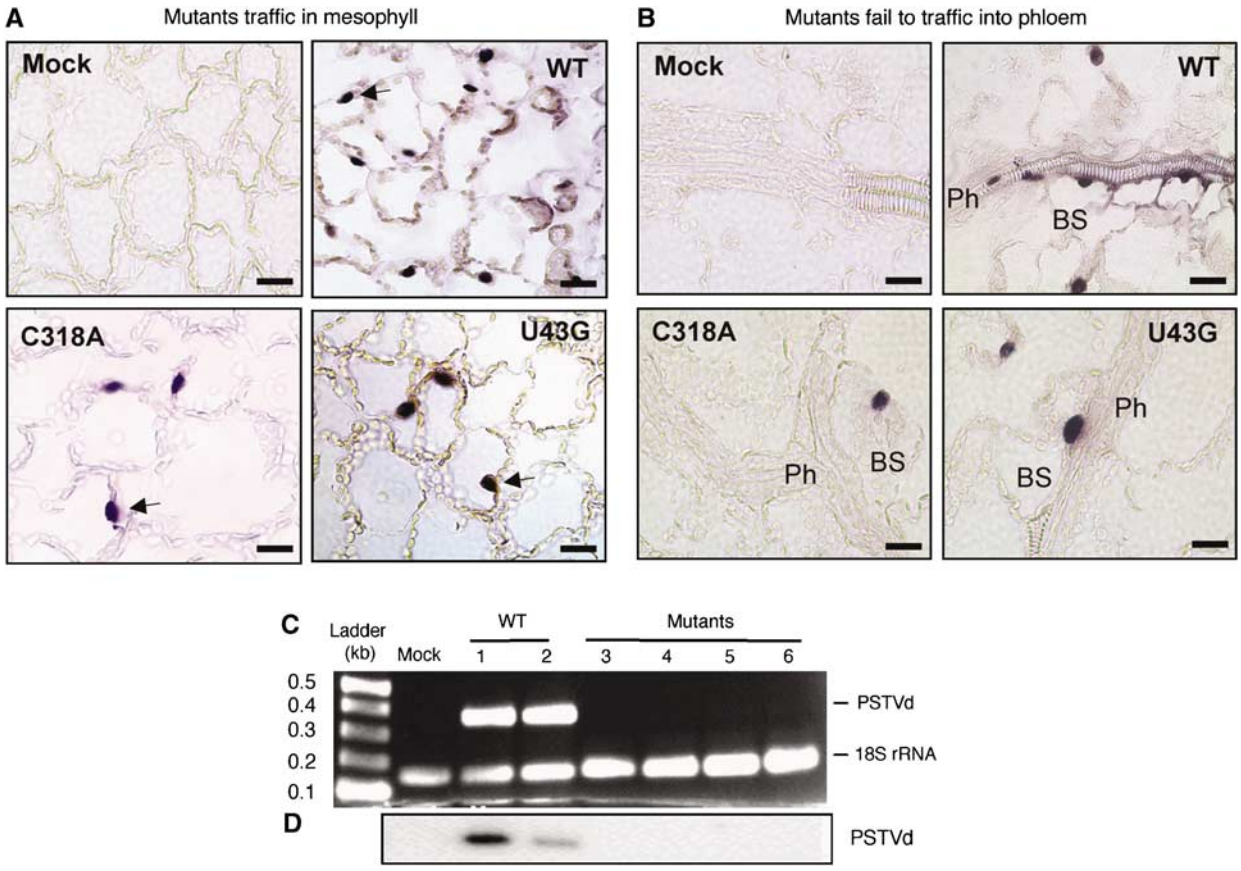

Figure 4 Mutants C318A and U43G fail to traffic into the vascular tissue phloem at 12 dpi. (**A**) *In situ* hybridization shows trafficking of the two mutants as well as the WT in mesophyll. The purple hybridization signals show the presence of viroid RNAs in the nuclei (arrows). There is no hybridization signal in mock-inoculated samples. (**B**) *In situ* hybridization shows trafficking of the two mutants as well as the WT into the bundle sheath (BS). While the WT also accumulates in the phloem (Ph), the two mutants are absent from the phloem. Scale bars, 10 μm. (**C**) RT–PCR detects the presence of WT PSTVd (lanes 1 and 2), but absence of mutants C318A (lanes 3 and 4) and U43G (lanes 5 and 6), in petioles of inoculated leaves. Amplification of 18S rRNA serves as an internal control. (**D**) Hybridization with a PSTVd-specific probe confirms identity of the RT–PCR products as PSTVd.

the detection limit of *in situ* hybridization. To test this possibility, we used the highly sensitive reverse transcription–polymerase chain reaction (RT–PCR) to detect the presence of mutants in the petioles of inoculated leaves at 12 dpi. As shown in Figure 4C, no signal was detected in any of the two plants infected by C318A or by U43G, whereas bands corresponding to the full-length PSTVd sequence could be detected in WT infection. Amplification of the 18S rRNA served as a control for the quality of RNA in each sample. Hybridization analysis with PSTVd-specific probes confirmed that the RT–PCR products indeed were PSTVd sequences (Figure 4D). Three repeated experiments yielded identical results.

Taken together, all data provided compelling evidence that mutants C318A and U43G had specific defects in entering the phloem from bundle sheath in *N. benthamiana* plants.

Predicted tertiary structure of U43/C318 motif

U43 and C318 are generally drawn unpaired in the secondary structure of PSTVd, forming a small 1 × 1 unpaired 'loop' flanked by *cis* Watson–Crick/Watson–Crick (cWW) base pairs as shown in Figure 1A and C. (In PSTVd, one of the flanking pairs is a G/U, which can form a cWW base pair nearly isosteric to cWW A/U or G/C, while in related viroids this pair is a G/C or A/U as shown in Supplementary Figure 4.) However, as shown by X-ray crystallography and nuclear magnetic resonance spectroscopy, most RNA 'loops' in structured, biologically active RNA molecules form distinct, well-structured three-dimensional (3D) motifs, in which most bases participate either in modified WW or non-WW base pairs and/or stacking interactions (Leontis *et al*, 2002). Many RNA 3D motifs are recurrent—they are observed in different RNA molecules (Leontis and Westhof, 2003; Leontis *et al*, 2006). Recurrent 3D motifs comprise sets of nucleotides with similar spatial arrangements and their 3D structures are generally more conserved than their sequences (Lescoute *et al*, 2005). On the basis of these considerations, we employed the 3D RNA motif search program, 'Find RNA 3D' or FR3D (Sarver *et al*, 2007), to search exhaustively the RNA 3D database for possible motifs formed by U/C base juxtapositions embedded in RNA helices so as to infer plausible tertiary structures for the PSTVd U/C motif.

The FR3D search revealed that in all cases the U and C bases were inserted in the helix, with their Watson–Crick edges facing each other and forming one or more hydrogen bonds (H-bonds). Moreover, for most occurrences in the highest-resolution X-ray crystal structures (<2.6 Å), the U and C bases form water-inserted *cis* WW (cWW) base pairs as shown in Figures 5 and 7. In this type of base pair, a direct H-bond exists between U(O4) and C(N4) and an inserted

water molecule forms bridging H-bonds with U(N3) and C(N3). The insertion of the water molecule opens the base pair toward the minor (shallow) groove of the RNA helix and significantly increases the C1′–C1′ distance from the normal ~10.6 Å of a canonical A/U or C/G cWW base pair to ~11.8 Å. The angle subtended by the glycosidic bonds of the U and C bases also increases. This causes a distortion of the helix, widening the minor groove locally as shown in Figure 5 when this helix is superimposed on a helix comprising exclusively canonical cWW base pairs. The latter was identified by a structure search using FR3D, in which the immediately flanking basepairs were matched to those of the U/C-containing helix. Based on these search results, we propose that U43 and C318 in the PSTVd 'loop' also form a cWW base pair with an inserted water molecule. The following analyses provide further evidence in support of this model.

Mutational analyses showed that local distortion of helix was critical for trafficking

To test whether the proposed local helix distortion is critical for trafficking, we generated all 16 possible nucleotide substitutions at positions 43 and 318 of PSTVd and tested their trafficking functions. We also carried out geometric structure searches using FR3D to identify exemplars in the 3D database for each mutant.

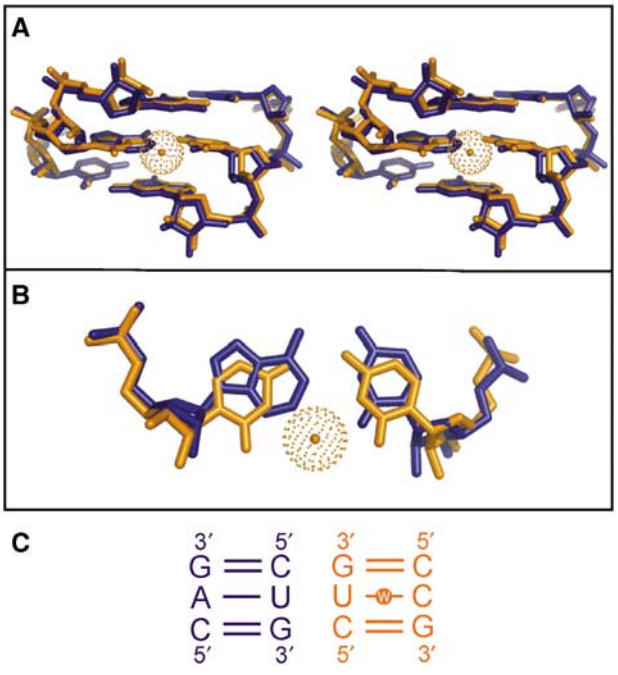

Figure 5 Local distortion of an RNA helix due to the presence of a water-inserted cWW U/C base pair. The X-ray crystal structure of an RNA helix containing a U/C water-inserted base pair (nucleotides 763:765 and 899:901 from PDB File: 1s72) is superimposed on a helix that contains matching cWW G/C flanking base pairs and cWW A/U in place of U/C (Nucleotides 444:446 and 36:38 from PDB file: 1s72). (**A**) A stereo figure showing the U/C-containing helix (orange), with the inserted water molecule shown as an orange sphere, superimposed on the helix 5′-CAG-3′/3′-GUC-5′ (blue; see panel C). (**B**) A planar view of the superimposition of the central water-inserted cWW U/C base pair (orange) on the cWW A/U base pair (blue). Insertion of the water opens the U/C base pair toward the minor groove, with little distortion of the neighboring base pairs. (**C**) Nucleotide sequences of the superimposed nucleotides.

The trafficking functions of all mutants are displayed in the 4 × 4 matrix in Figure 6A, based on their accumulation in systemic leaves as shown by RNA blots (Figure 6B). The green and red background colors denote base pairs that retained and lost systemic trafficking functions, respectively. Sequencing confirmed maintenance of the mutant sequences in the progeny. The first striking observation is that all nucleotide changes that allow formation of canonical cWW base pairs (AU, UA, GC and CG) abolished systemic accumulation. It should be noted that A43/U318 and C43/G318 did not show replication in protoplasts (lanes 4 and 15 in Figure 6C), so the current assay cannot determine whether they were truly defective in the trafficking function itself.

The G/G juxtaposition cannot form any type of cWW base pair. Consistent with this, the G43/G318 mutant is not viable in infection.

The C43/U318 substitution is viable in trafficking. It is expected to form a base pair that is very similar to U43/C318 (WT) due to symmetry as is evident in comparing the C/U and U/C panels in Figure 7. Sequence analysis of conserved C/U water-inserted base pairs in the rRNAs also revealed cases of C/U covarying with U/C, as discussed below.

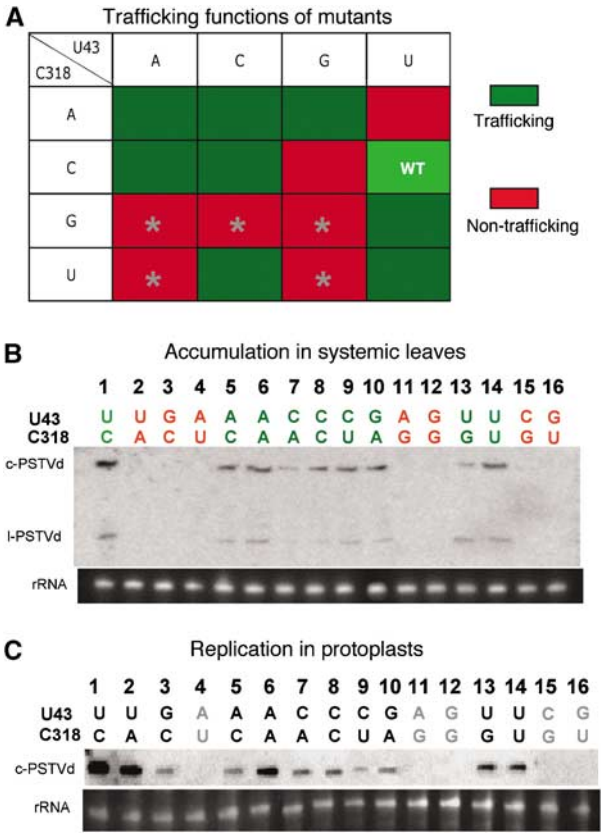

Figure 6 Mutational analyses of the trafficking motif. (**A**) A summary of mutagenesis results, with green and red boxes showing base pairs competent of and defective in systemic trafficking, respectively. Gray stars indicate mutants that do not replicate. WT indicates wild-type U43/C318 motif. (**B**) RNA blots showing presence or absence of the various mutants in systemic leaves of inoculated *N. benthamiana*. (**C**) RNA blots show presence or absence of the various mutants in inoculated *N. benthamiana* protoplasts. c-PSTVd, circular PSTVd; l-PSTVd, linear monomeric PSTVd. rRNA serves as loading controls.

The C43/C318 and U43/U318 substitutions are viable in trafficking. We used FR3D to search for C/C and U/U base pairs geometrically similar to the water-inserted U/C pair. The search revealed a similar C/C base pair also between two canonical cWW base pairs in the structure of an siRNA duplex bound to *Carnation Italian ringspot virus* P19 protein (PDB file: 1rpu) (Vargason *et al*, 2003). The protein-binding site spans the minor groove of the C/C base pair. The search also revealed a water-inserted cWW U/U base pair between two canonical cWW base pairs in the 16S rRNA A-site bound to Lividomycin A (PDB File: 2esj) (Francois *et al*, 2005). In this base pair, a direct H-bond exists between U5(O4) and U42(N3). An inserted water molecule forms bridging H-bonds with U5(N3) and U42(O2), opening the base pair toward the minor groove and increases the C1′–C1′ distance to 10.7 Å. Lividomycin binds in the major groove of the motif that includes the U/U base pair. Similar C/C and U/U base pairs occur in other structures and frequently have bound water molecules as shown in Figure 7. These pairs assume an asymmetric bifurcated geometry that also locally distort the helix, increasing the angle subtended by the glycosidic bonds of the bases and widening the minor groove with C1′–C1′ distances of ∼10.6 Å, longer than the ∼8.5 Å distance observed for 'wobble'-type cWW C/C or U/U base pairs.

G43/A318 is functional and can form a cWW base pair with a C1′–C1′ distance of 12.7 Å that also locally distorts the helix, as shown by the exemplar in Figure 7 (G150/A161 from PDB file 1hq1) (Batey *et al*, 2001). In contrast, the A43/G318 substitution does not show systemic accumulation. Because it fails to replicate (Figure 6C), its trafficking function cannot be determined. The A/G and G/A pairs are not completely symmetric structurally because A/G cWW base pairs tend to be propeller twisted and consequently the G(N2) amino group is not in the same place when the A and G are reversed (Sponer *et al*, 2003). The G(N2) functional group is most often observed to interact with protein in the minor groove. In the absence of an inserted water molecule available to interact with protein in the minor groove, the G(N2) functional group may play that role. Therefore, this additional level of interaction with different environments may render these two pairs functionally different (see further discussions below).

A43/A318 is viable for trafficking. Examples of A/A are observed forming cWW base pairs with a C1′–C1′ distance of 13.3 Å, as shown in Figure 7 (exemplar A675/A715 from 1j5e) (Wimberly *et al*, 2000). Thus A/A also distorts the helix by association with a water molecule in the minor groove.

G318/U43 is viable for trafficking. It is predicted to form a wobble cWW base pair as shown in Figure 7 (exemplar G226/U137 from 2avy) (Schuwirth *et al*, 2005) with a C1′–C1′ distance of 10.5 Å. G/U wobble pairs strongly bind a water molecule in the minor groove and present the G(N2)

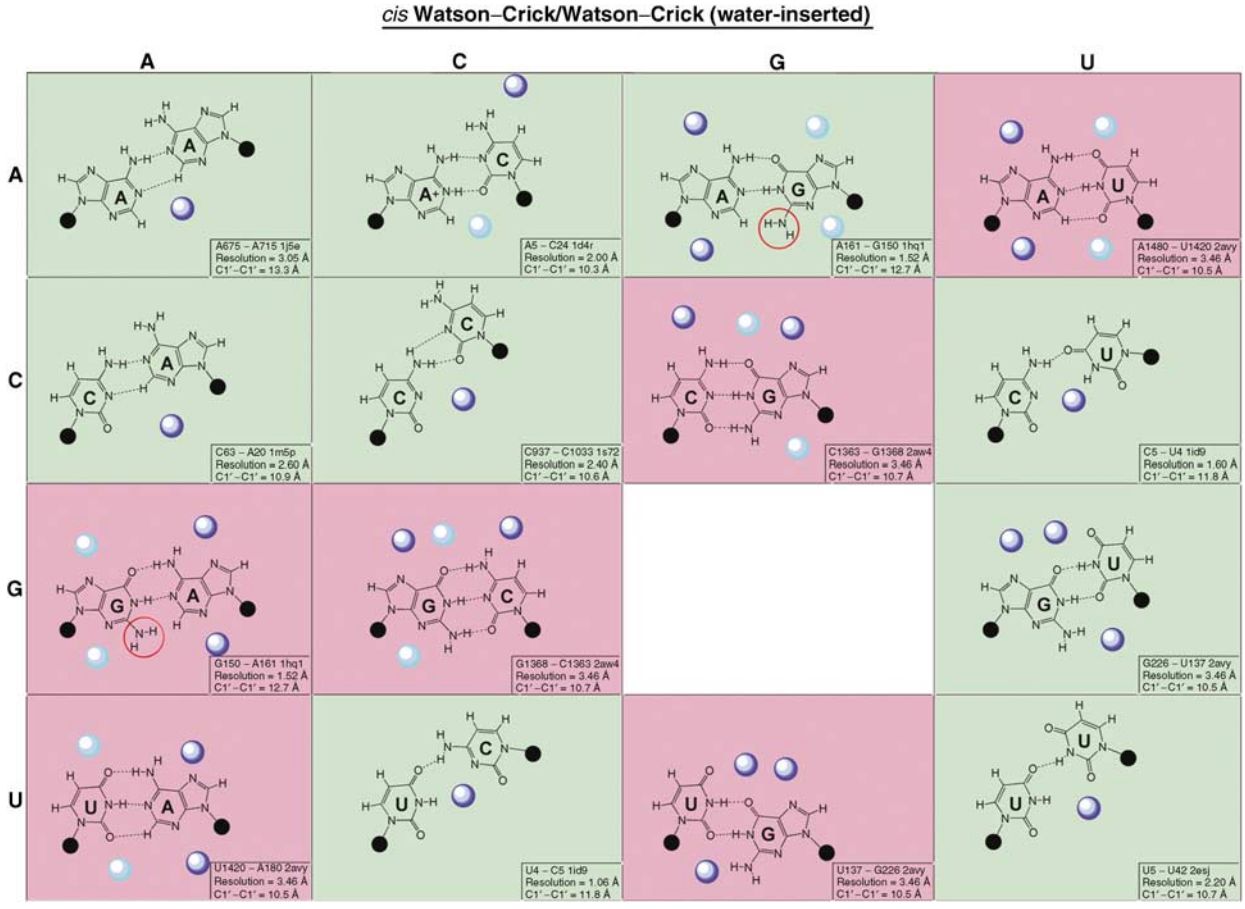

Figure 7 Hydration patterns for the cWW and water-inserted cWW base pairs. Dark blue and light blue spheres represent high-density and medium-density hydration sites identified on the Solvation Web Service site or by structure search using FR3D. Background colors correspond to the experimentally determined trafficking function.

functional group for possible interactions (Mokdad *et al*, 2006). G43/U318 is not viable likely for reasons similar to those for A43/G318.

A43/C318 and C43/A318 are both viable for trafficking. They are structurally similar to G318/U43 with C1′–C1′ distances of 10.3 and 10.9 Å, as shown in Figure 7 (exemplar A5/C24 from 1hq1 and C63/A20 from 1m5p) (Wild *et al*, 1999; Barton *et al*, 2002), and all can form a pocket that allows the insertion of water molecules to distort the helix.

The pattern that emerges from these analyses is that the mutations that did not disrupt the systemic trafficking function are all predicted to form modified cWW base pairs, some with inserted water molecules, that distort the helix and widen the minor groove, perhaps to facilitate interaction with a protein factor. In contrast, a regular helix without such distortion causes defects in systemic trafficking and possibly also replication for some base pairs.

Covariation analyses support the tertiary structural model

To further test our model, we performed two types of nucleotide covariation analyses, based on the rationale that when two nucleotides interact to form a particular structure, mutation in one nucleotide may result in covariation in its interacting nucleotide to maintain the same or similar structure and thus function (Pace *et al*, 1999). First, we examined the equivalent positions of other viroid sequences in the genus Pospiviroid that are predicted to fold into similar secondary structures as PSTVd. All of these viroids have the conserved loop E-like motif (Zhong *et al*, 2006). As shown in Figure 8 and Supplementary Figure 4, the U/C motif is conserved for *Tomato planta macho viroid* and *Tomato chlorotic dwarf viroid*, and is replaced by variation C/C in *Citrus exocortic viroid*, *Tomato apical stunt viroid* and *Chrysanthemum stunt viroid* and by variation A/A in *Mexican papita viroid* (Singh *et al*, 2003; Subviral RNA Database, http://subviral.med.uottawa.ca/cgi-bin/home.cgi). As discussed above, both A/A and C/C base juxtapositions in this context can form cWW base pairs with associated or inserted water molecules to distort the local helix (Figure 7), and are viable for trafficking (Figure 6).

We also performed covariation analyses of U/C base pairs in the structures of the rRNAs by using the Ribostral program for covariation analysis (Mokdad and Leontis, 2006). First, FR3D identified several U/C cWW base pairs in the 16S or 23S rRNA structures of *Escherichia coli* (Schuwirth *et al*, 2005) and *Thermus thermophilus* (Selmer *et al*, 2006), and in the 23S structure of *Haloarcula marismortui* (Harms *et al*, 2001). We focused our attention on those U/C pairs, which are flanked on both sides by canonical cWW base pairs (including G/U wobble) and which are conserved in two or more homologous structures. As shown in Figure 9, the three examples meeting these criteria are (1) U576/C565 in *E. coli* and *T. thermophilus* 23S (PDB files 2aw4 and 2j01); (2) U807/C673 in *E. coli* and *T. thermophilus* 23S and U900/C764 in *H. marismortui* 23S (PDB file 1s72); and (3) U2511/C2575 in *E. coli* and *T. thermophilus* 23S, which covary with U2546/U2610 in *H. marismortui* 23S. Interestingly, the first and third examples interact, at the widened minor groove, with the universally conserved proteins L3 and L4 that are crucial for 23S rRNA folding in the 50S ribosomal subunit (Klein *et al*, 2004). Second, sequence covariations were observed at

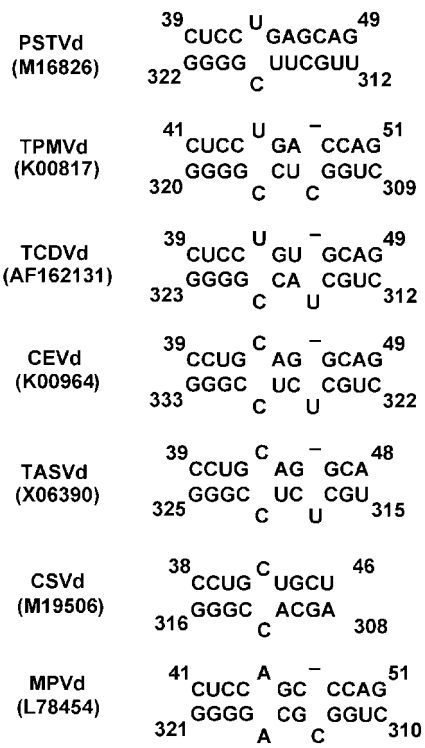

Figure 8 Covariation analyses of U/C motif in viroids of genus *Pospivitoid*, based on conservation of the overall secondary structures predicted by mfold. The analyses reveal conservation of U/C pair at the equivalent positions for *Tomato planta macho viroid* (TPMVd), *Tomato chlorotic dwarf viroid* (TCDVd), variation C/C for *Citrus Exocortic viroid* (CEVd), *Tomato apical stunt viroid* (TASVd) and *Chrysanthemum stunt viroid* (CSVd), and variation A/A for *Mexican papita viroid* (MPVd).

equivalent positions for these U/C pairs in 23S sequence alignments for bacteria (~800 sequences) and archaea (25 sequences) (Lescoute *et al*, 2005). As shown in Figure 9, for U576/C565 the primary covariation is C/U, while for U2511/C2575 it is U/U. Interestingly, U/U is observed at the corresponding position of the *H. marismonrtui* 23S structure and in the other archaeal sequences. All covariations of the U/C pair (i.e., C/U, U/U and U/G) in 23S are also functional in PSTVd (Figure 6), therefore supporting the structural model of the U/C pair.

Hydration patterns suggest a functional mechanism

For the reasons described above, we propose that the U/C base pair in the PSTVd forms a water-inserted cWW base pair with a widened minor groove conducive to protein and/or RNA interactions. To test this model, we examined the hydration patterns for all base juxtapositions that can form cWW or water-inserted cWW base pairs using the Solvation Web Service (SWS) (Auffinger and Hashem, 2007) in combination with geometric structure searches using FR3D. SWS provides solvation data for a given base pair type compiled from the entire structure database. SWS displays the solvation density surrounding each base pair type so that likely locations of water molecules can be inferred. In Figure 7 the dark blue spheres represent high density and the light blue spheres medium density solvation sites reported by SWS. For the pairs for which SWS did not yield such information (A/A, C/C, U/C, C/U), we employed FR3D to identify all examples

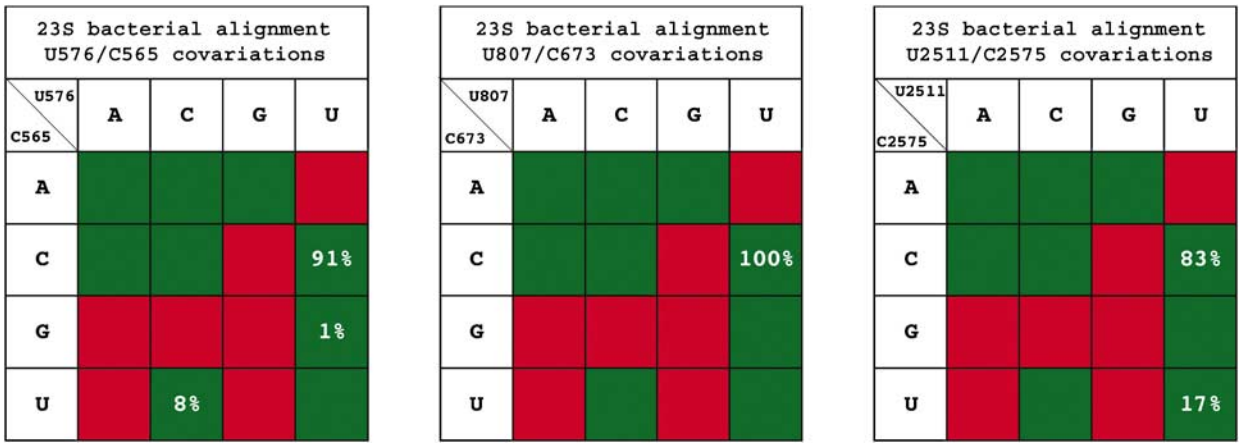

Figure 9 Covariation analysis for three conserved U/C base pairs found in 23S bacterial sequences. Nucleotide numbering is based on the *E. coli* sequence. The background colors indicate trafficking function in PSTVd variants for U43/C318.

in high-resolution X-ray crystal structures containing water molecules. For these pairs, the dark blue spheres indicate the sites of water molecules most often observed. Similar to Figure 6A, the green and red background colors in Figure 7 indicate base substitutions that are functional and defective in PSTVd trafficking, respectively. A clear pattern is that most functional base substitutions bind a water molecule using one or more Watson–Crick edges, resulting in opening of the base pair toward the minor groove. The only exception is A/G which has the G(N2) amino group occupying an equivalent position as an inserted water molecule. The G(N2) amino group is the most common site of protein binding in the minor groove (Klein *et al*, 2004), and examples involving A/G cWW pairs have been observed (Sponer *et al*, 2003).

Discussion

In this paper, we reported the first loss-of-function genetic identification of an RNA tertiary structural motif that is required for RNA trafficking from the bundle sheath into the phloem to initiate long-distance trafficking. This motif is not required for trafficking from epidermis to mesophyll and then to bundle sheath. Structurally, this motif comprises juxtaposed nucleotides U/C that form a water-inserted cWW base pair in a helical context, that is, flanked by cWW A/U, G/C or G/U base pairs. The fundamental feature of the motif is the local distortion of the helix caused by the U/C pair. This motif likely represents a protein-binding site, based on the known function of similar conserved motifs in other RNAs that interact with specific proteins. It is interesting that the left base pair C/G flanking the U/C motif in PSTVd, TPMVd and TCDVd changes to G/C when this motif is naturally replaced by C/C in CEVd, TASVd and CSVd. Whether these flanking sequences only support formation of a motif and/or whether they have functional significance in other capacities remains to be determined.

Although mutant U43G accumulates to lower levels than the WT PSTVd, our analyses of other mutants indicate that the viroid replication/accumulation levels are not a factor for cell-to-cell trafficking including vascular entry. For instance, the double mutants C43/U318 and G43/A318 (lanes 9 and 10, respectively, in Figure 6C) accumulate to lower levels than the WT (lane 1 in Figure 6C) in infected protoplasts, but they are competent in systemic trafficking (lines 9 and 10, respectively, in Figure 6B). Thus, the failure of mutants C318A and U43G, as well as other mutants, to traffic into the phloem most likely results from disrupted molecular interactions with a cellular factor(s) in the trafficking machinery.

The absence of mutants C318A and U43G in the phloem is unlikely attributed to their instability in the phloem. First, the secondary structure of PSTVd is resistant to RISC (RNA-Induced Silencing Complex)-mediated degradation (Wang *et al*, 2004; Itaya *et al*, 2007). C318A or U43G substitution causes only a mild change in the local but not the overall secondary structure of PSTVd. Therefore, it is unlikely that they will alter dramatically the stability of PSTVd. In fact, Owens *et al* (1996) showed that U43G substitution enhances the thermostability of PSTVd. Second, these mutants are stable and replicate in the protoplasts as well as epidermal, mesophyll and bundle sheath cells. There is no evidence yet that a special RNA degradation system exists in the phloem.

We previously showed that a bipartite motif in PSTVd is required for trafficking from bundle sheath to mesophyll, but is not required for trafficking from mesophyll to bundle sheath, in young tobacco leaves (Qi *et al*, 2004). We attempted to determine whether the U/C motif is required for trafficking from the phloem to bundle sheath by generating transgenic *N. benthamiana* plants expressing the cDNAs of C318A and U43G mutants under the control of a companion cell-specific promoter, thereby allowing primary transcripts derived from the promoter activity would serve as templates to initiate RNA–RNA replication (Qi *et al*, 2004). However, in all nine lines of transgenic plants viroid progeny showed reversion to WT sequences or mutations elsewhere (data not shown). Therefore, whether U/C or another motif is required for phloem exit remains to be determined. It also remains to be determined whether the U/C motif alone is sufficient or requires participation of another motif to mediate phloem entry.

It is unclear why certain nucleotide substitutions at U/C positions that distort the helix resulted in abolishment of replication. There are several possibilities. First, the U/C motif also plays a role in replication, besides phloem entry. The specific nucleotide substitutions, while maintaining similar structures as other replication-competent mutants, inhibit interactions with a cellular factor(s) important for

replication. There is precedence that a single viroid motif plays multiple roles and nucleotide identity is also important. For instance, the PSTVd loop E motif has a role in replication, host adaptation, *in vitro* processing and symptom expression (Ding and Itaya, 2007). Second, these nucleotide substitutions create a novel binding site for some cellular factors. Such binding results in mislocalization of the viroid RNAs within a cell or prevents access of the replication machinery. Resolving these issues should lead to new insights into the molecular interactions between an RNA motif and cellular factors.

The U/C motif may function in a host-specific manner. Owens *et al* (1996) showed that C318A did not affect systemic infection in tomato, consistent with our own observations (data not shown). On the other hand, U43G substitution affected systemic infection to some extent in tomato (Owens *et al*, 1996). Thus, vascular entry of PSTVd in tomato may involve an alternative mechanism. This is not surprising, considering the narrow host range of viroids and the observations that single nucleotide changes can alter host range (Wassenegger *et al*, 1996; Zhu *et al*, 2002) and host-dependent symptom expression (Qi and Ding, 2003). Consistent with our current study, Loss *et al* (1991) showed that C318G substitution did not affect systemic infection in tomato. It should be noted that a metastable hairpin II (HPII) structure has been postulated to play a critical role in PSTVd replication (Loss *et al*, 1991; Owens *et al*, 1991) and that U43G substitution presumably inhibits the formation of HPII (Owens *et al*, 1996). The normal replication of U43G in *N. benthamiana* raises the question whether this putative HPII plays a significant role in replication in this plant. The putative HPII unlikely has a role in trafficking, because C318A substitution has little effect on its formation.

Our data, together with previous work identifying a PSTVd motif for trafficking from bundle sheath to mesophyll (Qi *et al*, 2004), further support the hypothesis that the bundle sheath plays a critical role in regulating macromolecular trafficking between the phloem and non-vascular tissues. An emerging picture is that trafficking from the same cell into different neighboring cells involves different mechanisms. For instance, SUT1 mRNA is transported only from companion cells into sieve elements (Kühn *et al*, 1997). The identification of a viroid RNA motif for trafficking from the bundle sheath into phloem (this study), and a separate motif for trafficking from bundle sheath to mesophyll (Qi *et al*, 2004) provides the most compelling evidence that specific interactions between distinct RNA motifs and the yet-to-be identified cellular factors control trafficking of an RNA from the same cell into different neighbors. The cellular factors could be cytosolic factors and/or plasmodesmal components. This model should have important implications for the transport mechanisms of infectious and endogenous RNAs across various cellular boundaries.

The majority of studies on RNA functions rely on secondary structural analyses. In this study, we demonstrated the utility of a combination of 3D motif search, comparison with X-ray crystal structures, mutagenesis and covariation analysis to study the tertiary structure of a functional RNA motif. Our results, together with those from previous work using similar approaches to investigate the tertiary structure and function of another PSTVd motif (Zhong *et al*, 2006), provide compelling evidence that viroid RNAs share many structurally conserved motifs with other RNAs, and that they can be excellent models to investigate the general principles of RNA structure–function relationships. Furthermore, our approaches may be extended to investigate the structure–function relationships of other RNAs.

Materials and methods

Plant materials and growth condition

N. benthamiana plants were grown in a growth chamber maintained at 14 h light (27°C)/10 h dark (24°C) cycles. *N. benthamiana* cells were cultured in Murashige and Skoog medium (MS salts; Life Technologies, Rockville, MD). Cells were maintained and subcultured as previously described in Zhong *et al* (2006).

PSTVd cDNA construction

Plasmid pRZ6-2 containing cDNAs of $PSTVd^{Int}$ was constructed by Hu *et al* (1997) and was a gift from Dr Robert Owens. All PSTVd-derived mutants were generated by site-directed mutagenesis using the Quickchange Site-Directed Mutagenesis kit (Stratagene, La Jolla, CA) using pRZ:$PSTVd^{Int}$ as the template. The introduced mutations were verified by sequencing.

Construction of pInter(−) and pInter(+) is described in Qi and Ding (2002). *Spe*I-linearized pInter(−) and pInter(+) were used as the templates to generate riboprobes specific for (+) and (−)-PSTVd RNAs, respectively.

Plant and protoplast infection

The *in vitro* transcripts of PSTVd variants were used to inoculate the carborundum-dusted first two true leaves of 2-week-old *N. benthamiana* plants (300 ng/plant). DEPC-H_2O was used for mock inoculation. *N. benthamiana* protoplasts were prepared and transfected with PSTVd transcripts by electroporation, as described by Zhong *et al* (2006). At 3 dpi, transfected protoplasts were collected for RNA extraction and gel blot analysis.

In vitro transcription

To prepare riboprobes for RNA gel blots or *in situ* hybridization, α-^{32}P- or digoxigenin-UTP-labeled antisense riboprobes were prepared by *in vitro* transcription using T7 Maxiscript kit (Ambion, Austin, Texas, USA), following the methods recommended by the manufacturer, using *Spe*I-linearized pInter(−) or pInter(+) as the templates, respectively. After *in vitro* transcription, the DNA templates were removed by digestion with RNase-free DNase I. The RNA transcripts were purified with MEGAClear kit (Ambion) and were quantified by UV spectrometry or scintillation counting, respectively.

Tissue processing, in situ hybridization

Leaf samples were processed as described in Zhu *et al* (2001). Paraffin sections (8–10 μm) were obtained with a rotary microtome (HM340E, Microm International GmbH, Walldorf, Germany). *In situ* hybridization was performed as described previously (Qi *et al*, 2004), using digoxigenin-labeled antisense PSTVd riboprobes.

RNA extraction and RNA gel blot

Total RNAs from infected plants were isolated using Trizol reagent (Invitrogen, Carlasbad, CA, USA) and total RNAs from protoplasts were extracted using RNeasy plant mini kit (Qiagen, Valencia, California, USA) according to the manufacturer's instructions. RNA gel blots were performed as described in Zhong *et al* (2006).

RT–PCR

Total RNAs from *N. benthamiana* petioles were isolated using Trizol reagent (Invitrogen) and treated with TURBO DNA-free™ kit (Ambion), according to the manufacturer's instructions. A total of 1 μg of total RNA was reverse transcribed using the ThermoScript™ RT–PCR system (Invitrogen), using a reverse primer (5′-AGGAA CCAACTGCGGTTCCA-3′) for (+)-PSTVd and 1093-1114R (5′-CCCG GAACCCAAAAACTTTG-3′) for 18S rRNA. The reverse transcribed PSTVd cDNA was amplified by PCR with a forward primer (5′-CGG AACTAAACTCGTGGTTCCT-3′) and the reverse primer. The primers 1093-1114R and 1000-1020F (5′-GATCAGATACCGTCCTAGTC-3′) were used for amplification of 18S rRNA cDNA template, which served as an internal control. The PCR products were run on 1.2% agarose gel for EB staining, or 5% polyacrylamide/8 M urea gel for hybridization analyses using a riboprobe specific for PSTVd.

Sequencing of RNA progeny

The protocols for preparing cDNAs of the PSTVd progeny isolated from protoplasts or plants were performed essentially as described by Qi and Ding (2002). Briefly, cDNAs of PSTVd RNA were RT–PCR amplified and sequenced in both directions using the ABI377 DNA sequencer (Perkin-Elmer, Boston, MA) at the DNA Sequencing Facility at Ohio State University.

Supplementary data

Supplementary data are available at *The EMBO Journal* Online (http://www.embojournal.org).

Acknowledgements

We thank Ying Wang and Ryuta Takeda for assistance with some RNA hybridization experiments. We are indebted to Asuka Itaya for critical reading of the manuscript and insightful discussions. This work was supported by grants from the US National Science Foundation (IBN-0238412 and IOB-0620143 to BD) and National Institutes of Health (2R15GM055898-03 to NBL). Jesse Stombaugh is funded by NBL's RCE grant, which is supported by Bowling Green State University's 'Research Capacity Expansion Program' with funds provided by the Ohio Board of Regents Research Incentive Fund.

References

Auffinger P, Hashem Y (2007) SwS a solvation web service for nucleic acids. *Bioinformatics* **17:** 325–333

Banerjee AK, Chatterjee M, Yu Y, Suh SG, Miller WA, Hannapel DJ (2006) Dynamics of a mobile RNA of potato involved in a long-distance signaling pathway. *Plant Cell* **18:** 3443–3457

Barton WA, Biggins JB, Jiang J, Thorson JS, Nikolov DB (2002) Expanding pyrimidine diphosphosugar libraries via structure-based nucleotidylyltransferase engineering. *Proc Natl Acad Sci USA* **99:** 13397–13402

Batey RT, Sagar MB, Doudna JA (2001) Structural and energetic analysis of RNA recognition by a universally conserved protein from the signal recognition particle. *J Mol Biol* **307:** 229–246

Branch AD, Robertson HD (1984) A replication cycle for viroids and other small infectious RNAs. *Science* **223:** 450–455

Bucher G, Scholten J, Klingler M (2002) Parental RNAi in *Tribolium* (Coleoptera). *Curr Biol* **12:** R85–R86

Ding B (1998) Intercellular protein trafficking through plasmodesmata. *Plant Mol Biol* **38:** 279–310

Ding B, Itaya A (2007) Viroid: a useful model for studying the basic principles of infection and RNA biology. *Mol Plant Microbe Interact* **20:** 7–20

Ding B, Itaya A, Zhong X (2005) Viroid trafficking: a small RNA makes a big move. *Curr Opin Plant Biol* **8:** 606–612

Eiras M, Kitajima EW, Flores R, Daros JA (2007) Existence *in vivo* of the loop E motif in potato spindle tuber viroid RNA. *Arch Virol* **152:** 1389–1393

Fire A, Xu S, Montgomery MK, Kostas SA, Driver SE, Mello CC (1998) Potent and specific genetic interference by double-stranded RNA in *Caenorhabditis elegans*. *Nature* **391:** 806–811

Flores R, Hernandez C, Martinez de Alba AE, Daros JA, Di SF (2005) Viroids and viroid–host interactions. *Annu Rev Phytopathol* **43:** 117–139

Francois B, Russell RJ, Murray JB, boul-ela F, Masquida B, Vicens Q, Westhof E (2005) Crystal structures of complexes between aminoglycosides and decoding A site oligonucleotides: role of the number of rings and positive charges in the specific binding leading to miscoding. *Nucleic Acids Res* **33:** 5677–5690

Gross HJ, Domdey H, Lossow C, Jank P, Raba M, Alberty H, Sanger HL (1978) Nucleotide sequence and secondary structure of potato spindle tuber viroid. *Nature* **273:** 203–208

Hammond RW, Owens RA (1987) Mutational analysis of potato spindle tuber viroid reveals complex relationships between structure and infectivity. *Proc Natl Acad Sci USA* **84:** 3967–3971

Harms J, Schluenzen F, Zarivach R, Bashan A, Gat S, Agmon I, Bartels H, Franceschi F, Yonath A (2001) High resolution structure of the large ribosomal subunit from a mesophilic eubacterium. *Cell* **107:** 679–688

Haywood V, Kragler F, Lucas WJ (2002) Plasmodesmata: pathways for protein and ribonucleoprotein signaling. *Plant Cell* **14** (Suppl)**:** S303–S325

Haywood V, Yu TS, Huang NC, Lucas WJ (2005) Phloem long-distance trafficking of GIBBERELLIC ACID-INSENSITIVE RNA regulates leaf development. *Plant J* **42:** 49–68

Hu Y, Feldstein PA, Bottino PJ, Owens RA (1996) Role of the variable domain in modulating potato spindle tuber viroid replication. *Virology* **219:** 45–56

Hu Y, Feldstein PA, Hammond J, Hammond RW, Bottino PJ, Owens RA (1997) Destabilization of potato spindle tuber viroid by mutations in the left terminal loop. *J Gen Virol* **78:** 1199–1206

Itaya A, Zhong X, Bundschuh R, Qi Y, Wang Y, Takeda R, Harris AR, Molina C, Nelson RS, Ding B (2007) A structured viroid RNA serves as a substrate for dicer-like cleavage to produce biologically active small RNAs but is resistant to RNA-induced silencing complex-mediated degradation. *J Virol* **81:** 2980–2994

Kim M, Canio W, Kessler S, Sinha N (2001) Developmental changes due to long-distance movement of a homeobox fusion transcript in tomato. *Science* **293:** 287–289

Klein DJ, Moore PB, Steitz TA (2004) The roles of ribosomal proteins in the structure assembly, and evolution of the large ribosomal subunit. *J Mol Biol* **340:** 141–177

Kühn C, Franceschi VR, Schulz A, Lemoine R, Frommer WB (1997) Macromolecular trafficking indicated by localization and turnover of sucrose transporters in enucleate sieve elements. *Science* **275:** 1298–1300

Leontis NB, Lescoute A, Westhof E (2006) The building blocks and motifs of RNA architecture. *Curr Opin Struct Biol* **16:** 279–287

Leontis NB, Stombaugh J, Westhof E (2002) Motif prediction in ribosomal RNAs lessons and prospects for automated motif prediction in homologous RNA molecules. *Biochimie* **84:** 961–973

Leontis NB, Westhof E (2003) Analysis of RNA motifs. *Curr Opin Struct Biol* **13:** 300–308

Lescoute A, Leontis NB, Massire C, Westhof E (2005) Recurrent structural RNA motifs, isostericity matrices and sequence alignments. *Nucleic Acids Res* **33:** 2395–2409

Loss P, Schmitz M, Steger G, Riesner D (1991) Formation of a thermodynamically metastable structure containing hairpin II is critical for infectivity of potato spindle tuber viroid RNA. *EMBO J* **10:** 719–727

Lough TJ, Lee RH, Emerson SJ, Forster RL, Lucas WJ (2006) Functional analysis of the 5′ untranslated region of potexvirus RNA reveals a role in viral replication and cell-to-cell movement. *Virology* **351:** 455–465

Lough TJ, Lucas WJ (2006) Integrative plant biology: role of phloem long-distance macromolecular trafficking. *Annu Rev Plant Biol* **57:** 203–232

Lucas WJ (2006) Plant viral movement proteins: agents for cell-to-cell trafficking of viral genomes. *Virology* **344:** 169–184

Lucas WJ, Ding B, Van Der Schoot C (1993) Plasmodesmata and the supracellular nature of plants. *New Phytol* **125:** 435–476

Lucas WJ, Yoo BC, Kragler F (2001) RNA as a long-distance information macromolecule in plants. *Nat Rev Mol Cell Biol* **2:** 849–857

Mokdad A, Krasovska MV, Sponer J, Leontis NB (2006) Structural and evolutionary classification of G/U wobble basepairs in the ribosome. *Nucleic Acids Res* **34:** 1326–1341

Mokdad A, Leontis NB (2006) Ribostral: an RNA 3D alignment analyzer and viewer based on basepair isostericities. *Bioinformatics* **22:** 2168–2170

Owens RA, Chen W, Hu Y, Hsu YH (1995) Suppression of potato spindle tuber viroid replication and symptom expression by mutations which stabilize the pathogenicity domain. *Virology* **208:** 554–564

Owens RA, Steger G, Hu Y, Fels A, Hammond RW, Riesner D (1996) RNA structural features responsible for potato spindle tuber viroid pathogenicity. *Virology* **222:** 144–158

Owens RA, Thompson SM, Steger G (1991) Effects of random mutagenesis upon potato spindle tuber viroid replication and symptom expression. *Virology* **185:** 18–31

Pace NR, Thomas BC, Woese CR (1999) Probing RNA structure, function, and history by comparative analysis. In *The RNA World*, Gesteland RF, Cech TR, Atkins JF (eds) pp 113–141. New York, USA: Cold Spring Harbor Press

Palauqui JC, Elmayan T, Pollien JM, Vaucheret H (1997) Systemic acquired silencing: transgene-specific post-transcriptional silencing is transmitted by grafting from silenced stocks to non-silenced scions. *EMBO J* **16:** 4738–4745

Qi Y, Ding B (2002) Replication of Potato spindle tuber viroid in cultured cells of tobacco and *Nicotiana benthamiana*: the role of specific nucleotides in determining replication levels for host adaptation. *Virology* **302:** 445–456

Qi Y, Ding B (2003) Inhibition of cell growth and shoot development by a specific nucleotide sequence in a noncoding viroid RNA. *Plant Cell* **15:** 1360–1374

Qi Y, Pelissier T, Itaya A, Hunt E, Wassenegger M, Ding B (2004) Direct role of a viroid RNA motif in mediating directional RNA trafficking across a specific cellular boundary. *Plant Cell* **16:** 1741–1752

Qu F, Heinrich C, Loss P, Steger G, Tien P, Riesner D (1993) Multiple pathways of reversion in viroids for conservation of structural elements. *EMBO J* **12:** 2129–2139

Ruiz-Medrano R, Xoconostle-Cazares B, Lucas WJ (1999) Phloem long-distance transport of CmNACP mRNA: implications for supracellular regulation in plants. *Development* **126:** 4405–4419

Sarver M, Zirbel CL, Stombaugh J, Mokdad A, Leontis NB (2007) FR3D: finding local and composite recurrent structural motifs in RNA 3D structure. *J Math Biol* (in press)

Schuwirth BS, Borovinskaya MA, Hau CW, Zhang W, Vila-Sanjurjo A, Holton JM, Cate JH (2005) Structures of the bacterial ribosome at 3.5 Å resolution. *Science* **310:** 827–834

Selmer M, Dunham CM, Murphy FV, Weixlbaumer A, Petry S, Kelley AC, Weir JR, Ramakrishnan V (2006) Structure of the 70S ribosome complexed with mRNA and tRNA. *Science* **313:** 1935–1942

Singh RP, Ready KFM, Nie X (2003) Viroids of solanaceous species. In *Viroids*, Hadidi A, Flores R, Randles JW, Semancik JS (eds) pp 125–133. Collingwood, Australia: CSIRO

Sponer J, Mokdad A, Sponer JE, Spackova N, Leszczynski J, Leontis NB (2003) Unique tertiary and neighbor interactions determine conservation patterns of *cis* Watson–Crick A/G base-pairs. *J Mol Biol* **330:** 967–978

Vargason JM, Szittya G, Burgyan J, Tanaka Hall TM (2003) Size selective recognition of siRNA by an RNA silencing suppressor. *Cell* **115:** 799–811

Voinnet O, Baulcombe DC (1997) Systemic signalling in gene silencing. *Nature* **389:** 553

Voinnet O, Vain P, Angell S, Baulcombe DC (1998) Systemic spread of sequence-specific transgene RNA degradation in plants is initiated by localized introduction of ectopic promoterless DNA. *Cell* **95:** 177–187

Wang MB, Bian XY, Wu LM, Liu LX, Smith NA, Isenegger D, Wu RM, Masuta C, Vance VB, Watson JM, Rezaian A, Dennis ES, Waterhouse PM (2004) On the role of RNA silencing in the pathogenicity and evolution of viroids and viral satellites. *Proc Natl Acad Sci USA* **101:** 3275–3280

Wang Y, Zhong X, Itaya A, Ding B (2007) Evidence for the existence of the loop E motif of Potato spindle tuber viroid *in vivo*. *J Virol* **81:** 2074–2077

Wassenegger M, Heimes S, Sanger HL (1994) An infectious viroid RNA replicon evolved from an *in vitro*-generated non-infectious viroid deletion mutant via a complementary deletion *in vivo*. *EMBO J* **13:** 6172–6177

Wassenegger M, Spieker RL, Thalmeir S, Gast FU, Riedel L, Sanger HL (1996) A single nucleotide substitution converts potato spindle tuber viroid (PSTVd) from a noninfectious to an infectious RNA for *Nicotiana tabacum*. *Virology* **226:** 191–197

Wild K, Weichenrieder O, Leonard GA, Cusack S (1999) The 2 Å structure of helix 6 of the human signal recognition particle RNA. *Structure* **7:** 1345–1352

Wimberly BT, Brodersen DE, Clemons Jr WM, Morgan-Warren RJ, Carter AP, Vonrhein C, Hartsch T, Ramakrishnan V (2000) Structure of the 30S ribosomal subunit. *Nature* **407:** 327–339

Xoconostle-Cázarés B, Xiang Y, Ruiz-Medrano R, Wang HL, Monzer J, Yoo BC, McFarland KC, Franceschi VR, Lucas WJ (1999) Plant paralog to viral movement protein that potentiates transport of mRNA into the phloem. *Science* **283:** 94–98

Yoo BC, Kragler F, Varkonyi-Gasic E, Haywood V, Archer-Evans S, Lee YM, Lough TJ, Lucas WJ (2004) A systemic small RNA signaling system in plants. *Plant Cell* **16:** 1979–2000

Zhong X, Leontis N, Qian S, Itaya A, Qi Y, Boris-Lawrie K, Ding B (2006) Tertiary structural and functional analyses of a viroid RNA motif by isostericity matrix and mutagenesis reveal its essential role in replication. *J Virol* **80:** 8566–8581

Zhu Y, Green L, Woo YM, Owens R, Ding B (2001) Cellular basis of potato spindle tuber viroid systemic movement. *Virology* **279:** 69–77

Zhu Y, Qi Y, Xun Y, Owens R, Ding B (2002) Movement of potato spindle tuber viroid reveals regulatory points of phloem-mediated RNA traffic. *Plant Physiol* **130:** 138–146

Zuker M (2003) Mfold web server for nucleic acid folding and hybridization prediction. *Nucleic Acids Res* **31:** 3406–3415

